23. T. J. Coakley, "Turbulence modeling for the compressible Navier–Stokes equations," AIAA Paper N83-1693, New York (1983).
24. D. S. Dolling and C. T. Or, "Unsteadiness of the shock wave structure in attached and separated compression ramp flow fields," AIAA Paper N83-1715, New York (1983).

OPTICAL AND ACOUSTIC OBSERVATIONS OF STRATIFIED FLOW BEHIND A CYLINDER

V. E. Prokhorov, Yu. D. Chashechkin, and I. V. Voeikov

UDC 551.463.2+534.222

The shadow method, which gives highly sensitive measurements of the spatial and temporal structure of hydrophysical fields in one-component media, has been used successfully to visualize flows over experimental models. However, it is difficult to extract information on flow properties at an arbitrarily chosen point from the resultant integral picture.

The simplest method to make local measurements in a volume without perturbing it is to use remote pulsed soundings. The location and size of a specific volume can be specified by using time selection of the return signal. Ultrasonic hydrolocation (ultrasound location) is the most widely accepted pulsed sounding technique for natural causes (comparatively slow wave propagation, wavelength comparable to the inner flow scales). While it is widely used in medical diagnostics, ultrasonic location is poorly developed as an instrument for measuring the inner structure of hydrophysical fields.

The basic reason is the absence of a theoretical and empirical basis for constructing response functions which adequately describe the observed processes in terms a set of scattered acoustic signals, which in turn is explained by the transient nature of both the observed process and the scattered signals, as well as the inhomogeneity of the scatterer.

In order to establish a dependence between acoustic scattering and the flow conditions – and to identify the scatterer itself – ultrasonic soundings were made on flow behind a cylinder in water with a stratified salt concentration. The experiments were done in a tank (240 × 40 × 60 cm), which was equipped with an optical system (an IAB-458 shadow camera with a 23 cm view field), a conductometric profilometer, and a towing device for the cylinder.

The laboratory hydrolocator consisted of a receiver (a piezometric disk 2.5 cm in diameter), an output amplifier, an electronic pulse shaper, an echo signal preamplifier, a stroboscopic transformer, and a recorder. The stroboscopic transformer was required to scale the time in order to make the "fast" echo signals compatible with the inertial characteristics of the recorder. At the same time, shadow photographs were made of the flow field. The trigger signal for the camera was connected to the reference input of the recorder output.

The (salt concentration) was linearly stratified in a tank by a continuous extraction method. In these experiments, the buoyant frequency was $N = 0.6$ sec^{-1} [$N^2 = (g/\rho)d\rho/dz$, where ρ is the density, g is the acceleration due to gravity, and z is the vertical axis.] The cylinder diameter was $d = 5$ cm, the towing velocity varied from $u = 0.36$ cm/sec to 2.4 cm/sec, which corresponded to Froude numbers $Fr = u/Nd$ from 0.12 to 0.8 and Reynolds numbers $Re = ud/\nu$ from 180 to 1200 ($\nu \approx 0.01$ cm^2/sec).

Ultrasounding was done along the vertical with a repetition period of 10 msec of pulses of duration $\tau_0 = 20$ μsec and with a carrier frequency of 1 MHz (the ultrasonic wavelength was $\lambda = 0.15$ cm).

The cylinder is shown in the view field of the shadow camera in Fig. 1a (towing from left to right, $Fr = 0.67$, and $Re = 1000$). One can see the inner waves (the alternating light and dark vertical bands) ahead of the cylinder and elements of the nearby wake, including from the supporting blade, whose effects practically vanished with increasing time ($Nt > 5$).

Figure 1b illustrates the shape and location of the volume V which was irradiated with sound waves in the view field of the shadow camera. The droplet-shaped form of the volume

Moscow. Translated from Prikladnaya Mekhanika i Tekhnicheskaya Fizika, No. 3, pp. 68-74, May-June, 1993. Original article submitted April 10, 1992.

0021-8944/93/3403-0354$12.50

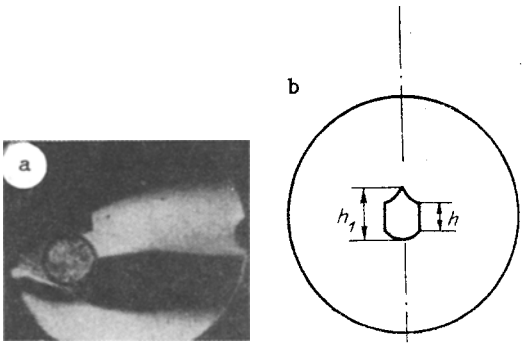

Fig. 1

is explained by the expansion of the leading and trailing wave fronts due to the resonance properties of the antenna. For the chosen repetition rate, the volume dimensions were h_1 = 2.2 cm, $h = c\tau_0/2$ = 1.5 cm (c = 0.15 cm/μsec is the sound speed), and the diameter of the horizontal cross section is roughly equal to the antenna diameter a = 2.5 cm, such that the average volume is $V_s = \frac{h_1 + h}{2}\frac{\pi a^2}{4} = S_a c\tau$, where $\tau = (h_1 + h)/c$, and S_a is the surface area of the antenna.

Figures 2-5 show movie frames of the wake and the corresponding echo records, the time axes of which show the time the photograph was recorded. The shadow structure behind the cylinder is formed by the near zone, which is described by the appropriate section of an Fr—Re diagram [1]. Each section corresponds to a specific set of hydrodynamic structures, one of which can carry the most energy.

Figure 2 shows an echo record (Fig. 2f) and a photograph for Fr = 0.8 and Re = 1200 at times Nt = 5, 7, 11, and 17 (Fig. 2a-2d), and also a shadow photograph for Fr = 0.12, Re = 180, and Nt = 5 (Fig. 3e). Towing is from left to right.

In this series of experiments, the outer wake dimensions are roughly identical at the limits of the range (Fr = 0.1, Re = 180) and (Fr = 0.8, Re = 1200); the flow has a microstructure in both cases (see photos in Fig. 2a and 2e). But at the lower boundary (Fig. 2e), the density-field structure in the view plane is a complex profile of isopycnic surfaces which vary slowly with time, while at the upper boundary (Fig. 2a) it is clearly turbulent. The difference in pulse rate can even be seen visually (Fig. 2a is more diffuse than Fig. 2e). The difference in the level of the echo signals is very notable in Fig. 5a, which shows a family of curves of the scattering coefficient $n = A_s/A_i\eta$ as a function of the Froude number (A_s and A_i are the amplitudes of scattered and radiating signals, and η = 0.066 is the efficiency of the echo locator) for wake increments at Nt = 7, 15, 21, 32, 43 (points 1-5). It can be seen that the value n(0.12) is an order of magnitude less than n(0.8) on the average. However, this does not mean that the scattering intensity has a direct dependence on Fr. As Fr increases, the echo signal grows monotonically only to Fr = 0.35, after which the function n(Fr) starts to oscillate (Fig. 5a).

Figure 3 shows the echo record (Fig. 3e) and the wakes (towing from right to left for Fr = 0.61 and Re = 910 at times Nt = 14, 19, 31, and 45 (Fig. 3a-3d), and Fig. 4 shows pictures of the wakes (towing direction is shown by arrows) at times Nt = 3 (Fig. 4a, 4c, and 4e) and Nt = 21 (Fig. 4b, 4d, and 4f) for Fr = 0.26 and Re = 385 (Fig. 4a and 4b), Fr = 0.67 and Re = 1000 (Fig. 4c and 4d), and Fr = 0.73 and Re = 1100 (Fig. 4e and 4f) and echo records for Fr = 0.26 and Re = 385 (Fig. 4g) and Fr = 0.67 and Re = 1000 (Fig. 4h).

Intercomparison of the echo and the shadow records shows that, first, the greatest scattering is observed under conditions where the flow has a microstructure, such as for Fr = 0.26 (Fig. 4a and 4b), Fr = 0.67 (Fig. 4c and 4d), and Fr = 0.8 (Fig. 2a-2d). Conversely, conditions with a predominant large-scale structure, where Fr = 0.61 (Fig. 3) and Fr = 0.73 (Fig. 4e and 4f), show weak scattering, in spite of a large number of surfaces with a density of discontinuity in the wake. Second, among the flows with a rich microstructure, the maximum scattering occurs in those where the rate of microscale pulsations is the largest.

In this regard, a plausible scattering mechanism is that the acoustic contrast is formed due to the transport of liquid particles into nonequilibrium density levels. Here the current

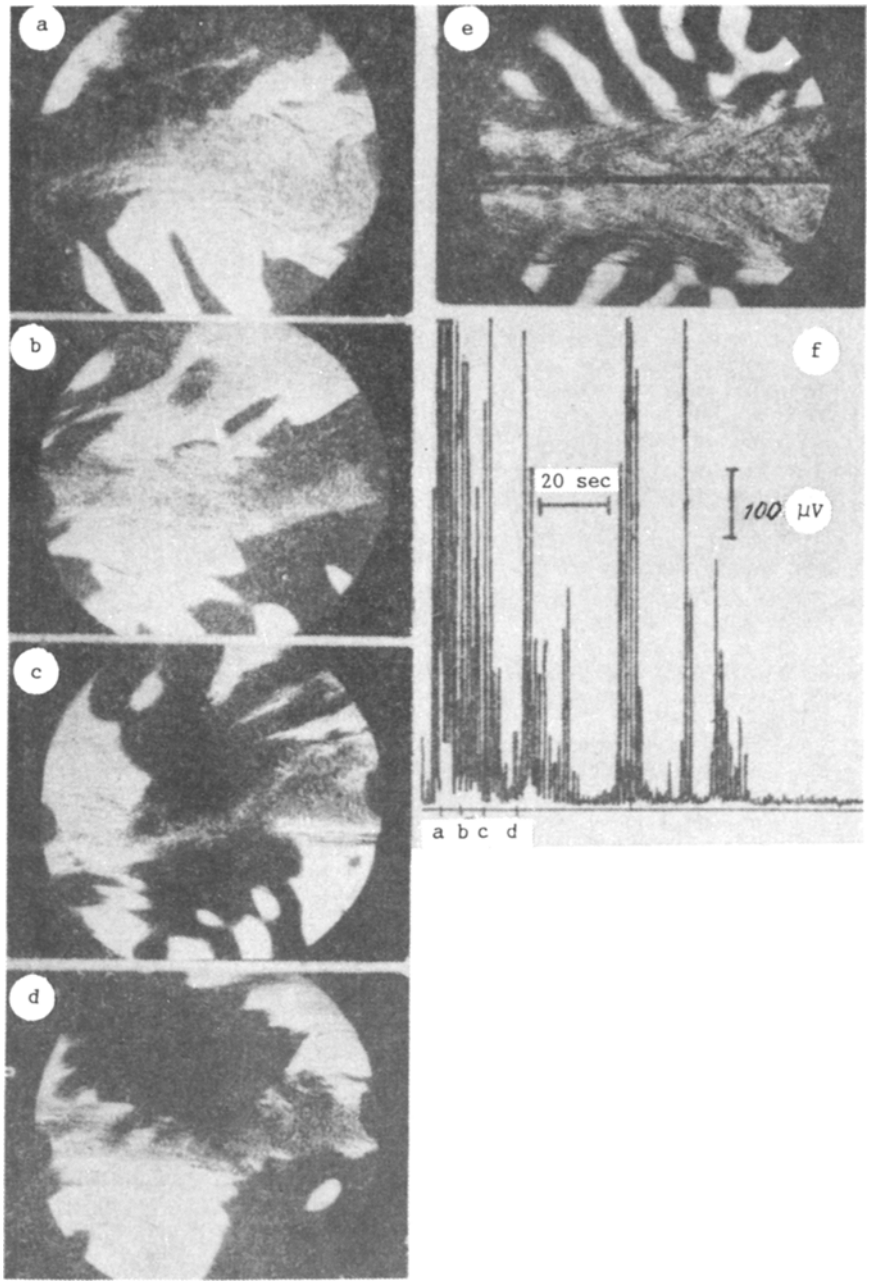

Fig. 2

particle concentration (and along with it the amount of scattering) is determined by the frequency at which they appear in these levels, that is by the pulsation rate. Because the difference in physical properties which create the acoustic contrast is formed when particles are transported in the field of an average gradient to a height ℓ, which in essence is a pulsation scale, the problem becomes one of relating this scale to the echo signal parameters.

From the viewpoint of the theory of scattering on discrete particles, the following situations can occur:

1. $k\ell/2 \ll 1$, where $k = 2\pi/\lambda$. If the scale ℓ is assumed to be much less than the buoyancy scale, the microscale nonuniformities take the form of spheres of radius $\ell/2$. Then, by assuming that small pulsations with an adiabatic compressibility $\varkappa'$ and density ρ' are created on a scale of ℓ in the gradient field of the average values of $\varkappa$ and ρ, the back-scattering cross section for a single particle can be easily obtained from Rayleigh's formula [2]:

$$\sigma = \frac{2}{3}(kl/2)^4(1 - 2\beta_\varkappa/\beta_\rho)(l/2\Lambda)(l/2)^2,$$

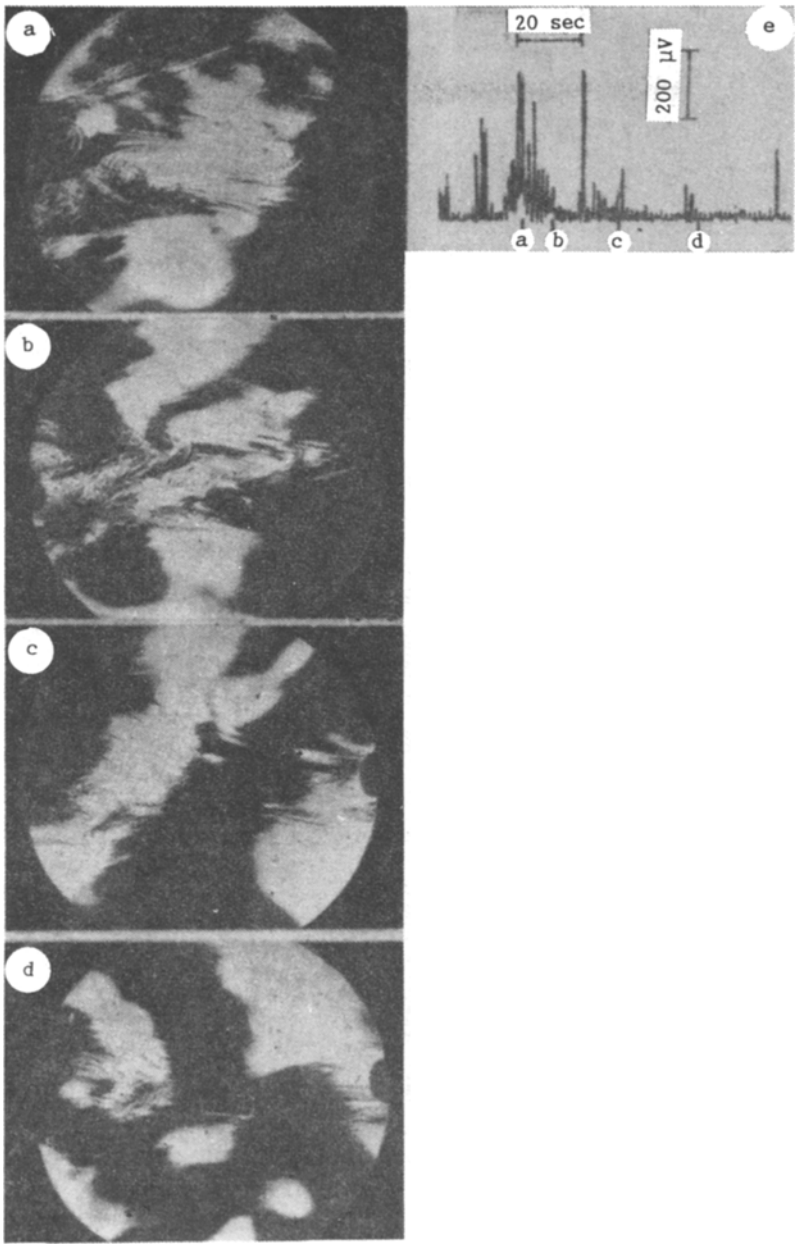

Fig. 3

where $\beta_\varkappa = \frac{1}{\varkappa}\frac{\partial \varkappa}{\partial S} \approx -2.23\cdot 10^{-3}\,(^0/_{00})^{-1}$; $\beta_\rho = \frac{1}{\rho}\frac{\partial \rho}{\partial S} \approx 0{,}84\cdot 10^{-3}\,(^0/_{00})^{-1}$; S is the salinity, ‰; $\Lambda = q/N^2$ is the stratification scale.

The scattering cross section can easily be related to the echo signal parameters via a volumetric scattering cross section m_V by the equation

$$m_v = \mu\sigma, \quad m_v = P_s/I_i V_s = n^2(c\tau/2).$$

Here μ is the volumetric concentration of the scatterers; $P_S = A_S^2$ is the scattering rate; $I_i = A_i^2/S_a$ is the intensity of the incoming wave. Because the volume of a single scatterer is $V_0 = \pi\ell^3/6$, the volumetric scattering coefficient can be expressed in terms of the alternation coefficient $\Gamma = \mu V_0$ (that is, the ratio of the volume of the perturbed liquid fraction to the volume V_S of scatterers in the same volume):

$$m_v = \Gamma(kl/2)^4\Lambda^{-1}.$$

If $k\ell/2 \ll 1$, the upper limit of the volumetric scattering coefficient in this approximation is reached when $k\ell/2 \sim 0.1$. Assuming that the maximum value is $\Gamma = 0.5$ (estimates are less than 0.2-0.3 [3]), we obtain

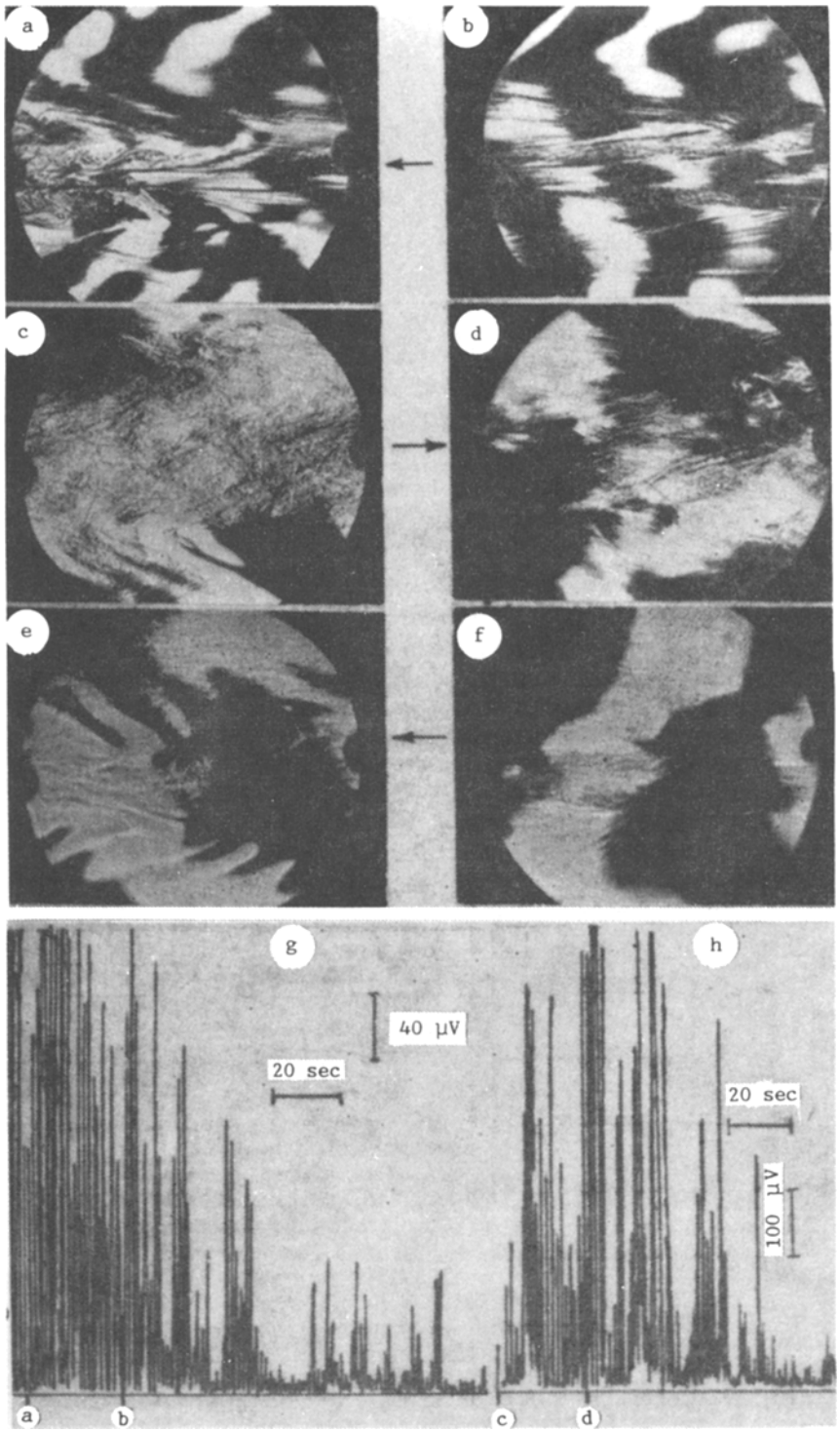

Fig. 4

$$m_v < 3{,}7 \cdot 10^{-9}\ \text{cm}^{-1}.$$

for our stratification ($\Lambda = 2.7 \cdot 10^3$ cm). Figure 5b shows m_V as a function of Fr for wake increments at Nt = 7, 15, 21, 32, and 43 (points 1-5). It can be seen that its measured values are several orders of magnitude above the theoretical estimate, which leads to the conclusion that there is no Rayleigh scattering at small scales.

2. $k\ell/2 \geq 1$. This is the case of geometric scattering at scales $\ell \geq \lambda/\pi$, which gives a basis to introduce a reflection coefficient ξ from the surface of the scatterer on which there is a jump r' in the acoustic impedance $r = \rho c$:

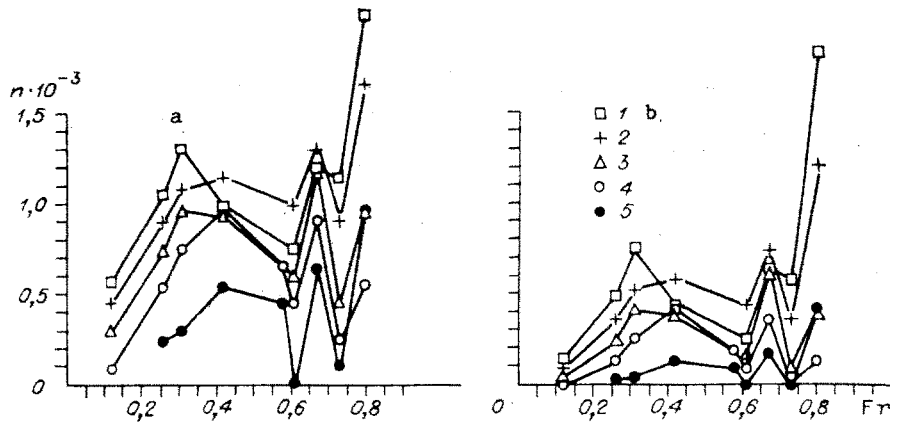

Fig. 5

$$\xi = r'/2r = (\rho'/\rho - \varkappa'/\varkappa)/4.$$

With one-component stratification and an average salinity gradient γ_S, the density and compressibility pulsations have the form $\rho'/\rho = \gamma_S\beta_\rho\ell$ and $\varkappa'/\varkappa = \gamma_s\beta_\varkappa l$, so that $\xi = (1 - \beta_\varkappa/\beta_\rho)l/4\Lambda$. Then the recordable power of the antenna from single-particle scattering is $P_{s0} = \xi^2 I_i S_a$ and the total power is $P_S = \mu V_S P_{S0}$. Because $0.5\mu\ell^3 \approx \Gamma$, then

$$m_V = \frac{2\Gamma}{l}\left(\frac{1 - \beta_\varkappa/\beta_\rho}{4}\right)^2 \Lambda^{-2} S_a.$$

In the case of inverse scattering of a plane wave, there is a known relationship between the volumetric scattering coefficient and the three-dimensional spectrum $\Phi(k)$ of the index of refraction in the form $m_V = 2\pi k^4 \Phi(2k)$, according to which this contribution to the scattering has a scale $\ell_r = \lambda/2$ (Bragg resonance). The problem of the resonance scale magnitude in the near zone of an acoustic field (the case here) remains open because the plane-wave approximation is not applicable. However, it is natural to expect a resonance interaction, even under laboratory conditions. Therefore the last formula shows the path for measuring the alternation coefficient from the back-scattering signal:

$$\Gamma = B m_V l_r \Lambda^2 \left(B = \frac{1}{2}\left(\frac{1 - \beta_\varkappa/\beta_\rho}{4}\right)^{-2} S_a^{-1}\right).$$

In this sense the experimental curves $m_V(Fr)$ in Fig. 3b are a scaled representation of the function $\Gamma(Fr)$.

For example, by assuming that $\ell_r = \lambda/2 = 0.075$ cm in our experiments, we obtain an alternation coefficient $\Gamma = 0.07$ for an average value $m_V = 10^{-6}$ cm^{-1} for a scatterer concentration of

$$\mu = \Gamma/V_0 = 2\Gamma/l_r^3 \approx 3 \cdot 10^2 \text{ cm}^{-3}.$$

Thus, the experimental data lead to the conclusion that the basic scattering source is a microstructural inhomogeneity, so that the scattering intensity is directly related to the intensity of the pulsations. With time, the continuous microstructure wake decays into separate regions which, by participating in the wave motions, periodically enter the acoustic irradiation zone. This explains the discontinuous nature of the echo records (Fig. 4). This behavior occurs for small towing velocity (Fr < 0.35), when the length $2\pi dFr$ of the attached inner wave is still comparable with the linear dimensions of the irradiated volume. Further growth in Fr leads to a change in flow conditions and structures.

The start of the range (Fr = 0.12 and Re = 180) corresponds to conditions of microscale instability (Fig. 2e); as Fr increases this instability transforms to a chain of suspended vortical dipoles at Fr = 0.26 (the vortical wakes can be seen in Fig. 4a and 4b in the form of concentrated layers), and then it transforms to turbulent-wake conditions at Fr = 0.8. The microscale structures, which are good scatterers, arise under these conditions. However, the existence of sharp drops in the echo record at Fr = 0.61 and 0.73 indicate that within this range there are intermediate conditions with a very different flow structure, which is confirmed by the shadow photographs (Figs. 3e, 3f, 4e, and 4f). Thus, the combined use of acoustic and optical methods makes it possible to refine the picture of the conditions and to obtain local characteristics of the evolving flow structures.

LITERATURE CITED

1. D. L. Boyer, P. A. Davies, H. Fernando, and X. Zhahg, "Linearly stratified flow past a horizontal circular cylinder," Phil. Trans. R. Soc. London A, 328, 501 (1989).
2. J. V. Rayleigh, The Theory of Sound, Dover, New York (1945).
3. Yu. M. Lytkin and G. G. Chernykh, "Similarity of flow according to the Froude density number and the energy balance during the evolution of a turbulent mixing zone in a stratified medium," in: Dynamics of Continuous Media, a Collection of Scientific Papers, Siberian Branch of the Academy of Sciences, Institute of Hydrodynamics [in Russian], Vol. 47 (1980).
4. L. A. Chernov, Waves in Randomly Inhomogeneous Media [in Russian], Nauka, Moscow (1975).